Available online at www.sciencedirect.com

ScienceDirect

journal homepage: www.elsevier.com/locate/he

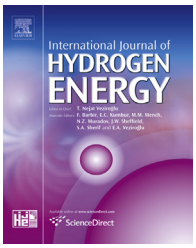

Kinetic analysis of H_2 addition effect on the laminar flame parameters of the C1–C4 n-alkane-air mixtures: From one step overall assumption to detailed reaction mechanism

Yu Cheng, Chenglong Tang, Zuohua Huang**

State Key Laboratory of Multiphase Flow in Power Engineering, Xi'an Jiaotong University, Xi'an 710049, People's Republic of China

ARTICLE INFO

Article history:
Received 3 September 2014
Received in revised form
27 October 2014
Accepted 2 November 2014
Available online 24 November 2014

Keywords:
Laminar flame speed
Hydrogen addition
One step overall reaction assumption
Detailed kinetic effect

ABSTRACT

In this work, numerical simulations on the laminar premixed C1–C4 n-alkanes with various hydrogen addition fractions (X_h) were conducted. Flame parameters, including laminar flame speed, adiabatic flame temperature (T_{ad}), flame thickness (δ_l), Lewis number (*Le*), Zeldovich number (*Ze*) and Markstein number (*Ma*) were calculated. Results show that hydrogen addition alters all flame parameters, especially at the sufficiently large X_h region. Based on one step overall reaction assumption, the hydrogen addition effect is demonstrated through three factors and it was found that the change in overall activation energy which represents the combustion kinetics, is the most prominent, compared to the change in adiabatic flame temperature and Lewis number. Detailed flame structure profiles show that the laminar flame speeds of all mixtures are linearly correlated with the maximum (H + OH) mole fraction and increase with X_h. To further understand the chemical kinetic effect of hydrogen addition on the increase of laminar flame speed, the reaction flux and rate of consumption of key radicals were examined. It is shown that at the small X_h region, the proportion of H radical consumption from R88 (CH_3+H(+M) = CH_4(+M)) increases, while the proportion of H radical consumption from R1 (H + O_2 = O + OH) decreases, thus relatively less OH radicals are produced. As a consequence, the increase in laminar flame speeds by hydrogen addition is slowed down. While at the large X_h region, the proportion of H radical consumption from R88 decreases dramatically, and the chain sequence R12 (H + O_2(+M) = HO_2(+M))/R16 (HO_2 + H = OH + OH) which is not sensitive at small X_h region is activated and significant amount of OH radicals are generated, leading to the remarkable increase of the laminar flame speed.

* *Corresponding authors.*
E-mail addresses: chenglongtang@mail.xjtu.edu.cn (C. Tang), zhhuang@mail.xjtu.edu.cn (Z. Huang).
http://dx.doi.org/10.1016/j.ijhydene.2014.11.010

Introduction

Due to the growing demand of oil supply and the concerns over the atmospheric pollution, there have been significant interests in the renewable and clean energy sources and the high efficiency combustion techniques for the internal combustion engines in the past decades. Hydrogen is one of the most promising alternative fuels because of its high flame speed, wide flammability limits and low ignition energy [1–5]. Additionally, the burning of hydrogen yields no greenhouse gas emissions. However, pure hydrogen burning in engines is also challenged by high level of NO_x emissions because of its high flame temperature. Additionally, pure hydrogen burning causes the issue of pre-ignition because of its low ignition energy, wide flammability limits and short quenching distance. At present, a widely used alternative fuel for the spark ignition engine as well as for gas turbine is natural gas. The components of natural gas depend on the production site, but the main component is methane, along with smaller amounts of heavier hydrocarbons such as ethane, propane, butane, and even pentane [6]. Although the natural gas has been widely used in a variety of combustion devices, it does have some unfavorable combustion characteristics, such as the slow flame speed and poor lean-burn capability, resulting in low thermal efficiency, large cycle-by-cycle variation and decreased engine power output, compared to gasoline. Thus using hydrogen as an additive to hydrocarbon fuels to increase the overall hydrogen-to-carbon ratio is a more practical approach. The high flame speed, wide flammability range, low ignition energy, high diffusivity and low emissions of hydrogen burning have drawn much attention and extensive studies have been conducted on internal combustion engines fueled by hydrogen-natural gas mixtures [7–10]. Additionally, there has been a growing interest in the ultra-lean nature gas burning in gas turbines to achieve the ultra-low NO_x emissions. One issue concerning the lean natural gas burning in gas turbine is that the flames are prone to be unstable, which can potentially lead to the system failure [11]. Thus the concept of hydrogen enriched combustion technique was proposed because the lean stability limits will be extended with the addition of hydrogen. Thus understanding the fundamental mechanisms of the hydrogen enriched combustion is important.

Fundamentally, previous studies on hydrogen enriched alkane or natural gas have been widely reported in ignition delay times [12–17] and laminar flame speeds [18–32]. Among all the fundamental parameters in combustion, laminar flame speed is one of the most important ones because it is benchmark data for the turbulent flame speed correlation. Furthermore, the laminar flame speed can be used to validate the chemical reaction mechanisms. Up to now, a number of fundamental studies on hydrogen enriched alkane fuel have been reported. These studies include binary fuels of hydrogen with methane [18–26], ethane [27], propane [18,19,28,29] and n-butane [30,31].

Previous studies on hydrogen enriched combustion used different definitions of hydrogen addition extent. The hydrogen mole fraction definition (X_h) is straightforward and have been used frequently [21–26,28,32] and these studies show that a weak increase of flame speed is observed when

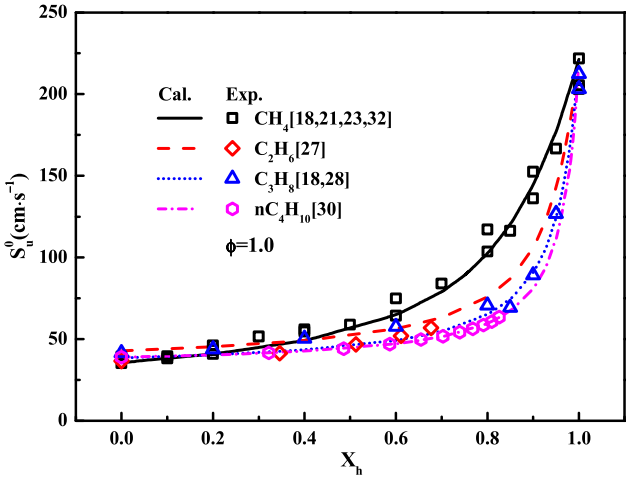

Fig. 1 – Comparison of experimental and calculated laminar flame speeds of C1–C4 n-alkane-hydrogen-air mixtures at 1 atm and 298 K: symbols for experimental data [18,21,23,27,28,30,32] and lines for calculation using USC Mech II.[35].

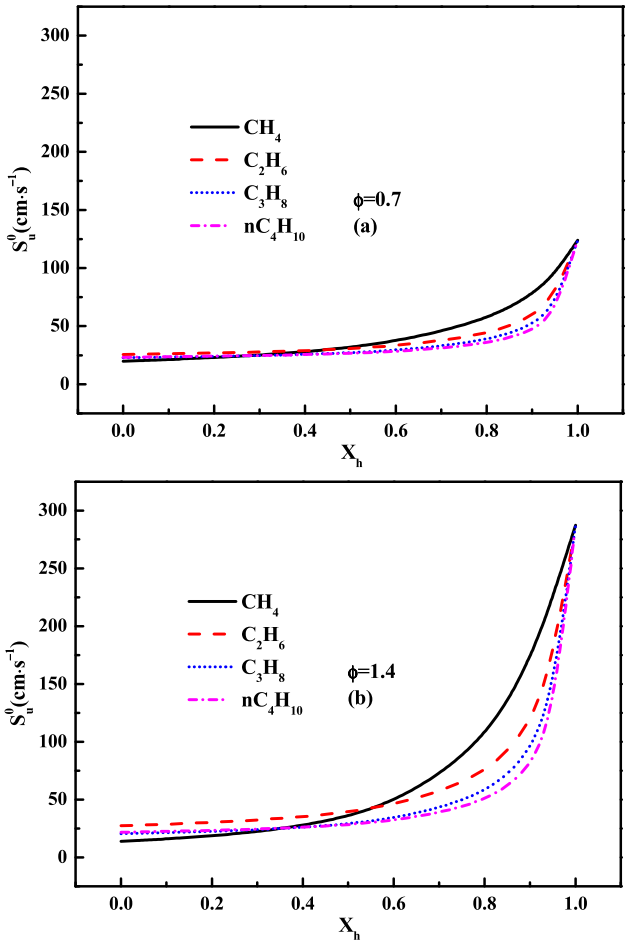

Fig. 2 – Calculated laminar flame speeds of C1–C4 n-alkane-hydrogen-air mixtures versus X_h at 1 atm and 298 K. (a) $\phi = 0.7$; (b) $\phi = 1.4$.

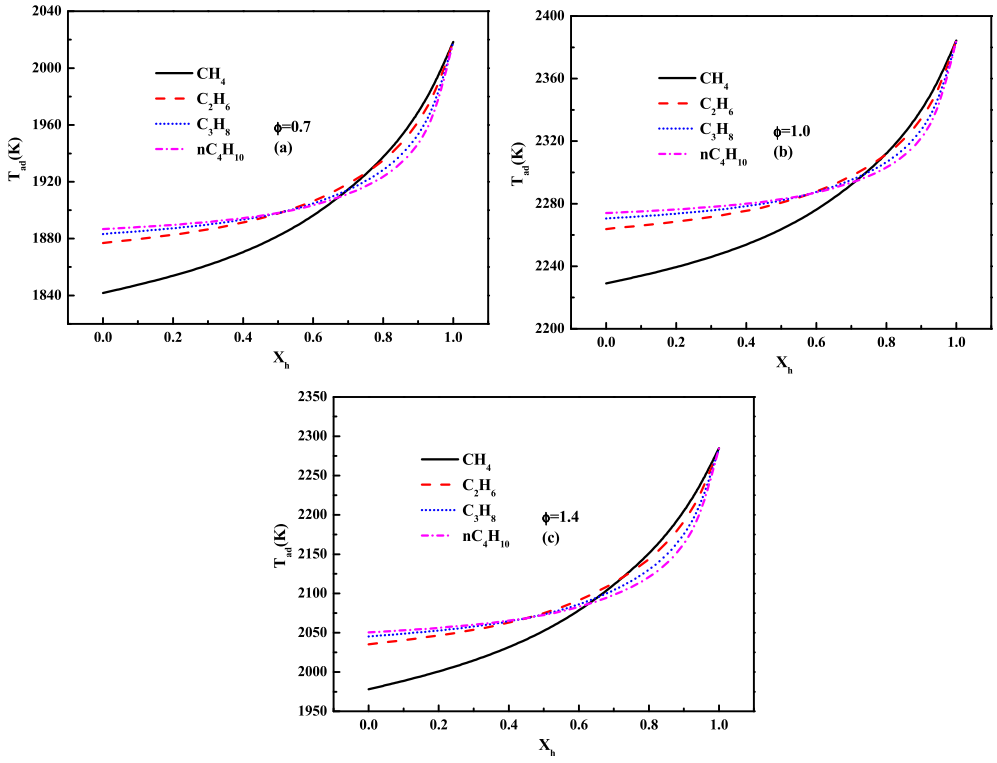

Fig. 3 – Calculated adiabatic flame temperature of C1–C4 n-alkane-hydrogen-air mixtures versus X_h at 1 atm and 298 K. (a) $\phi = 0.7$; (b) $\phi = 1.0$; (c) $\phi = 1.4$.

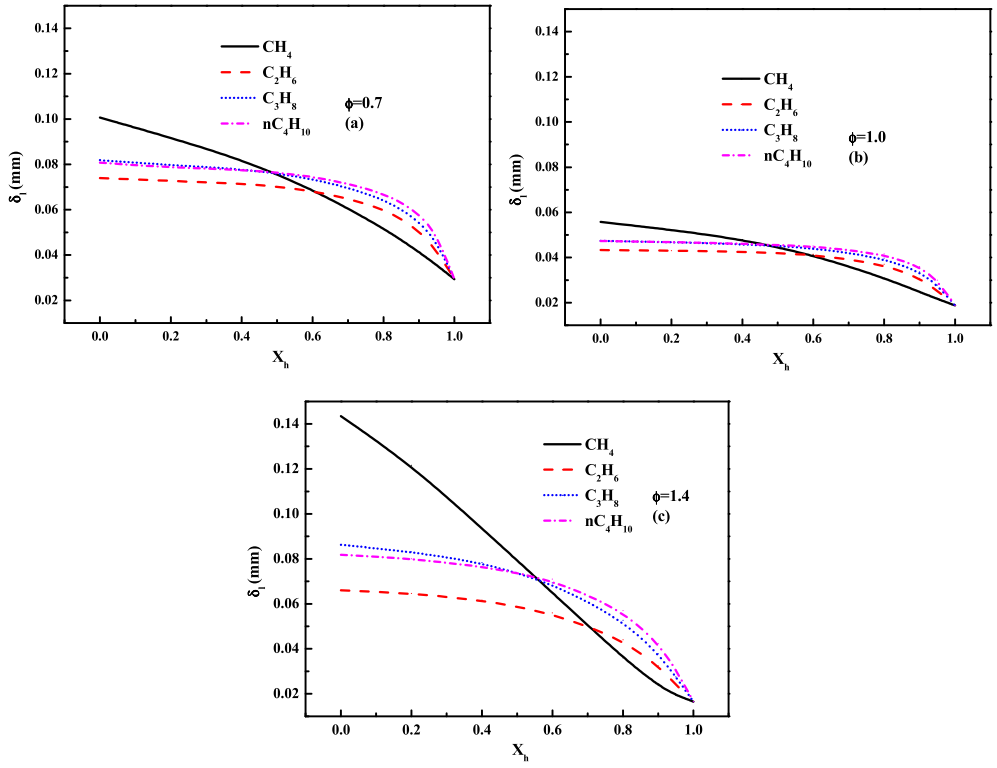

Fig. 4 – Calculated flame thickness of C1–C4 n-alkane-hydrogen-air mixtures versus X_h at 1 atm and 298 K. (a) $\phi = 0.7$, (b) $\phi = 1.0$, (c) $\phi = 1.4$.

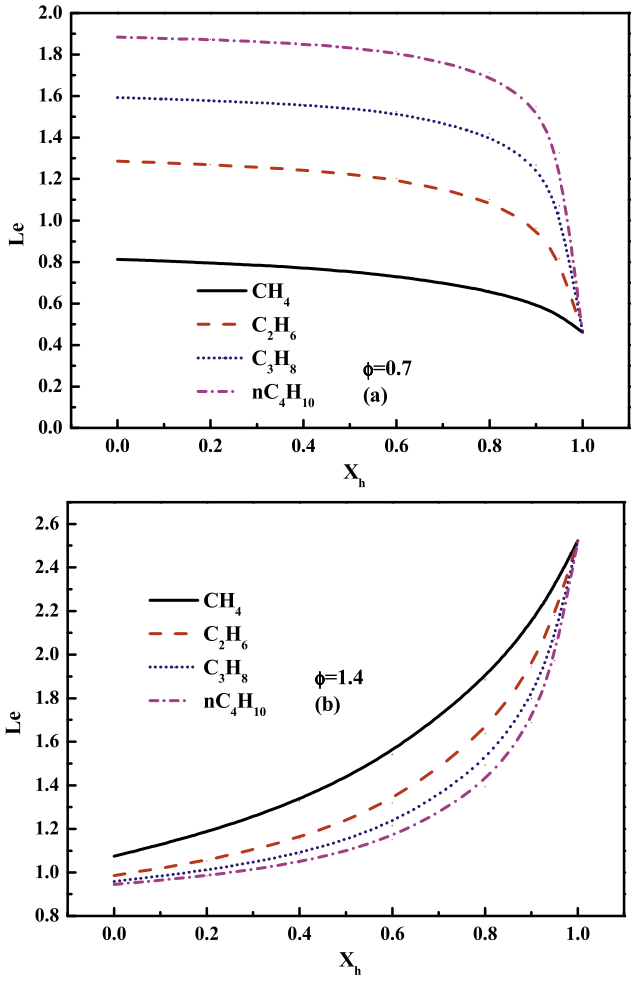

Fig. 5 – Calculated Lewis number of C1–C4 n-alkane-hydrogen-air mixtures versus X_h at 1 atm and 298 K. (a) $\phi = 0.7$; (b) $\phi = 1.4$.

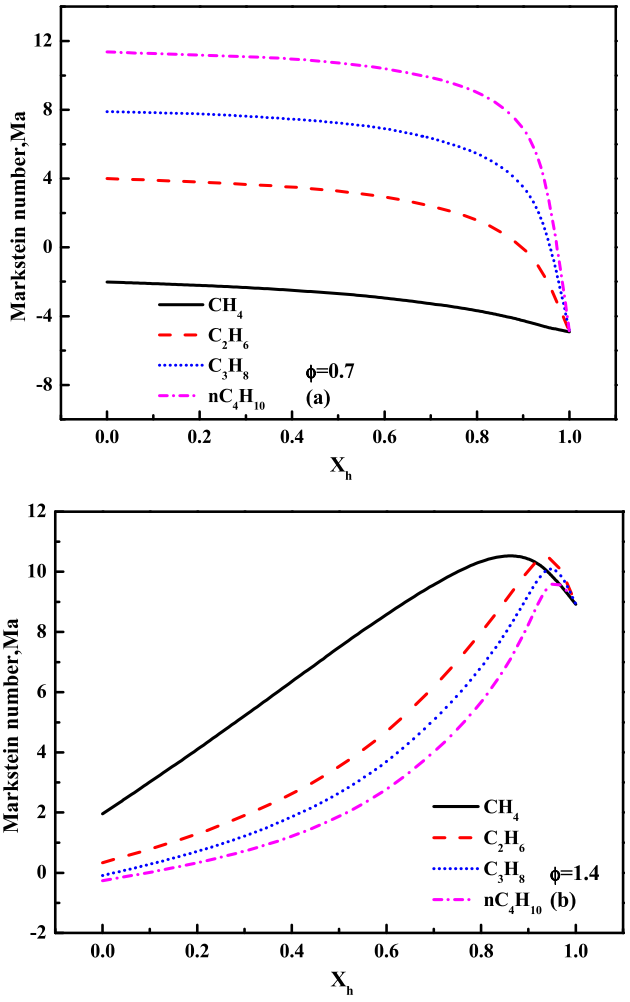

Fig. 7 – Calculated Markstein number of C1–C4 n-alkane-hydrogen-air mixtures versus X_h at 1 atm and 298 K. (a) $\phi = 0.7$; (b) $\phi = 1.4$.

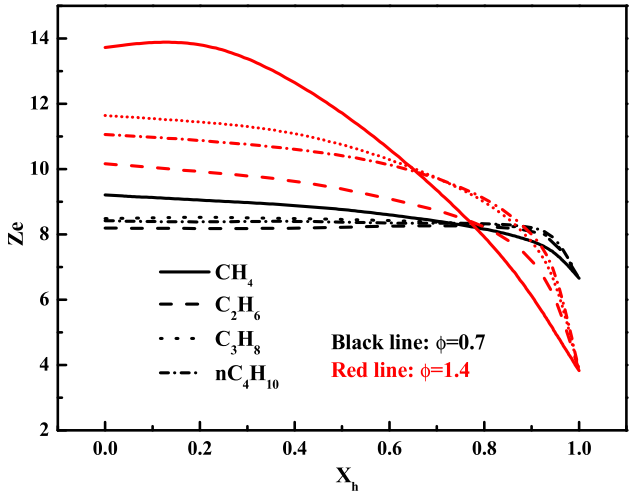

Fig. 6 – Calculated Zeldovich number of C1–C4 n-alkane-hydrogen-air mixtures versus X_h with different equivalence ratios at 1 atm and 298 K.

hydrogen fractions in fuels are small (less than 40%) but when hydrogen fractions are high enough (more than 80%), there is a sharp increase in flame speed. The other definition of the hydrogen addition extent is proposed by Yu et al. [19], who assumed that the stoichiometrically small amounts of hydrogen in the mixture were completely consumed and a hydrogen addition extent R_H is defined. Later studies by Wu [27], Sher [31] and Tang [30] used the same definition and the flame speed is found to be linearly correlated with the defined hydrogen addition parameter R_H.

Although much research has been devoted to the laminar flame speeds of the alkane–hydrogen blends, the fundamental understanding of the flame enhancement effect by hydrogen addition still remains to be systematically explored, and the underlying physics of the nonlinear dependence of laminar flame speed on hydrogen mole fraction needs to be further interpreted. One objective of this study is to present the dependences of the premixed flame parameters of gaseous alkane (methane, ethane, propane and n-butane)-air mixtures with hydrogen addition. These parameters include laminar

flame speed (S_u^0), adiabatic flame temperature (T_{ad}), flame thickness (δ_l), Lewis number (*Le*), Zeldovich number (*Ze*) and Markstein number (*Ma*), etc. The available measurements of these parameters will be compared with numerical simulations by using the PREMIX codes in conjunction with the CHEMKIN package. Additionally, based on the one step overall reaction assumption, the laminar flame speed can be correlated with the Lewis number (*Le*), the adiabatic flame temperature (T_{ad}) and the overall activation energy (E_a), which respectively demonstrate the transport, the thermal and the kinetic effect. Our second objective is to clarify the modification of these three mechanisms due to hydrogen addition. Finally, we note that the overall activation energy is only a global flame parameter derived from the one step overall reaction assumption and its dependence on X_h does not represent the real modification of the oxidation kinetics due to hydrogen addition, thus the chemical kinetic analysis will be conducted.

Numerical approach

Mechanism

Laminar flame speeds of C1–C4 n-alkane-air mixtures with hydrogen addition were calculated at 298 K and 1 atm at equivalence ratios of 0.7, 1.0, and 1.4, using the PREMIX codes combined with the CHEMKIN packages [33,34]. In this study, mixture-averaged diffusivity model was employed and Soret effect was not considered. The USC Mech II [35], which contains 111 species and 784 reactions, was employed for the simulation.

The hydrogen addition level is represented by the hydrogen fraction in the total fuel mixtures, and is defined as.

$$X_h = \frac{C_H}{C_H + C_A} \tag{1}$$

where C_A and C_H are the mole fractions of the alkanes and hydrogen, respectively.

Fig. 1 compares the measured [18,21,23,27,28,30,32] and numerically predicted laminar flame speeds of C1–C4 n-alkane-hydrogen-air mixtures at 1 atm and 298 K. The calculated laminar flame speeds show good agreement with the reported experimental ones, indicating the validity of the mechanism.

Flame parameters

The flame thickness in this work is defined as [36,37]

$$\delta_l = (\lambda/C_p)/(\rho_u S_u^0) \tag{2}$$

where λ, C_p and ρ_u are thermal conductivity, specific heat and density of the unburned gas mixture, respectively.

The Lewis number, *Le*, is expressed as:

$$Le = \alpha/D_m = \lambda/(\rho_u C_p D_m) \tag{3}$$

where $\alpha = \lambda/(\rho_u C_p)$ represents the thermal diffusivity of the mixtures and D_m is the mass diffusivity of the deficient reactant to the abundant inert. For the fuel lean conditions, the deficient reactants are the fuel mixtures, and the effective Lewis number is calculated as [36]

$$Le = 1 + \frac{q_{H_2}(Le_{H_2} - 1) + q_{Alkane}(Le_{Alkane} - 1)}{q_{H_2} + q_{Alkane}} \tag{4}$$

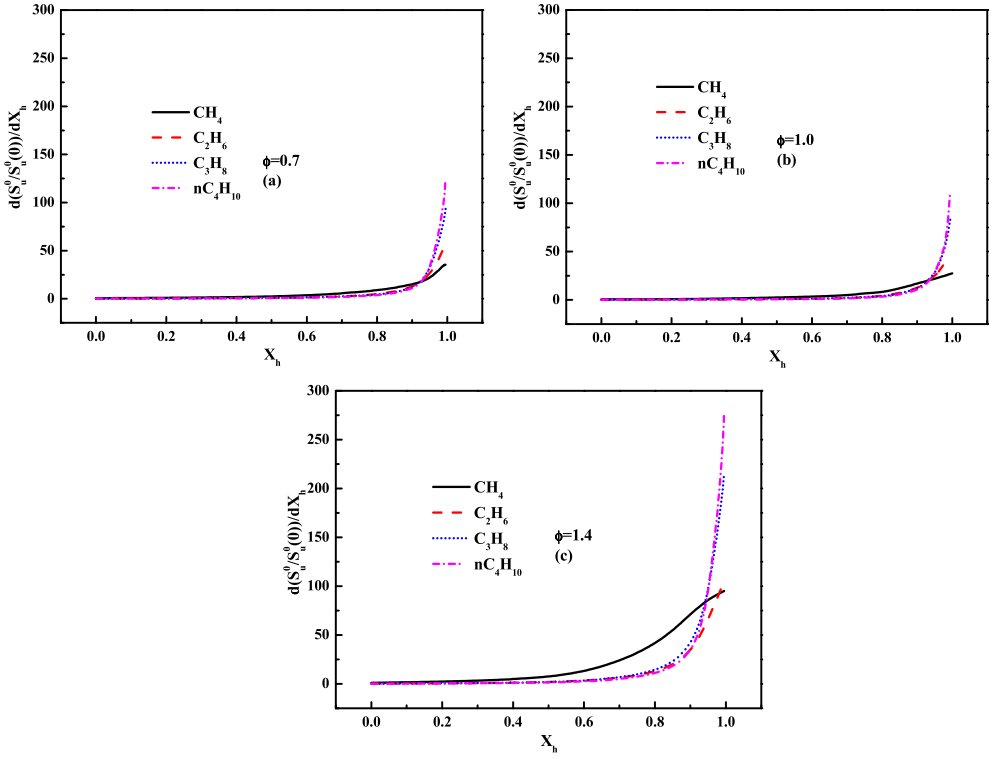

Fig. 8 – Calculated growth rates of the normalized laminar flame speeds of C1–C4 n-alkane-hydrogen-air mixtures versus X_h at 1 atm and 298 K. (a) $\phi = 0.7$; (b) $\phi = 1.0$; (c) $\phi = 1.4$.

where Le_i and q_i are the Lewis number and the dimensionless heat release rate of the ith species (i = hydrogen and alkanes), respectively.

Based on the one step overall reaction assumption, the Zeldovich number, is calculated as.

$$Ze = \frac{E_a(T_{ad} - T_u)}{RT_{ad}^2} \quad (5)$$

For sufficiently off-stoichiometric mixtures, E_a can be determined through the following equation, as suggested by Law [38]

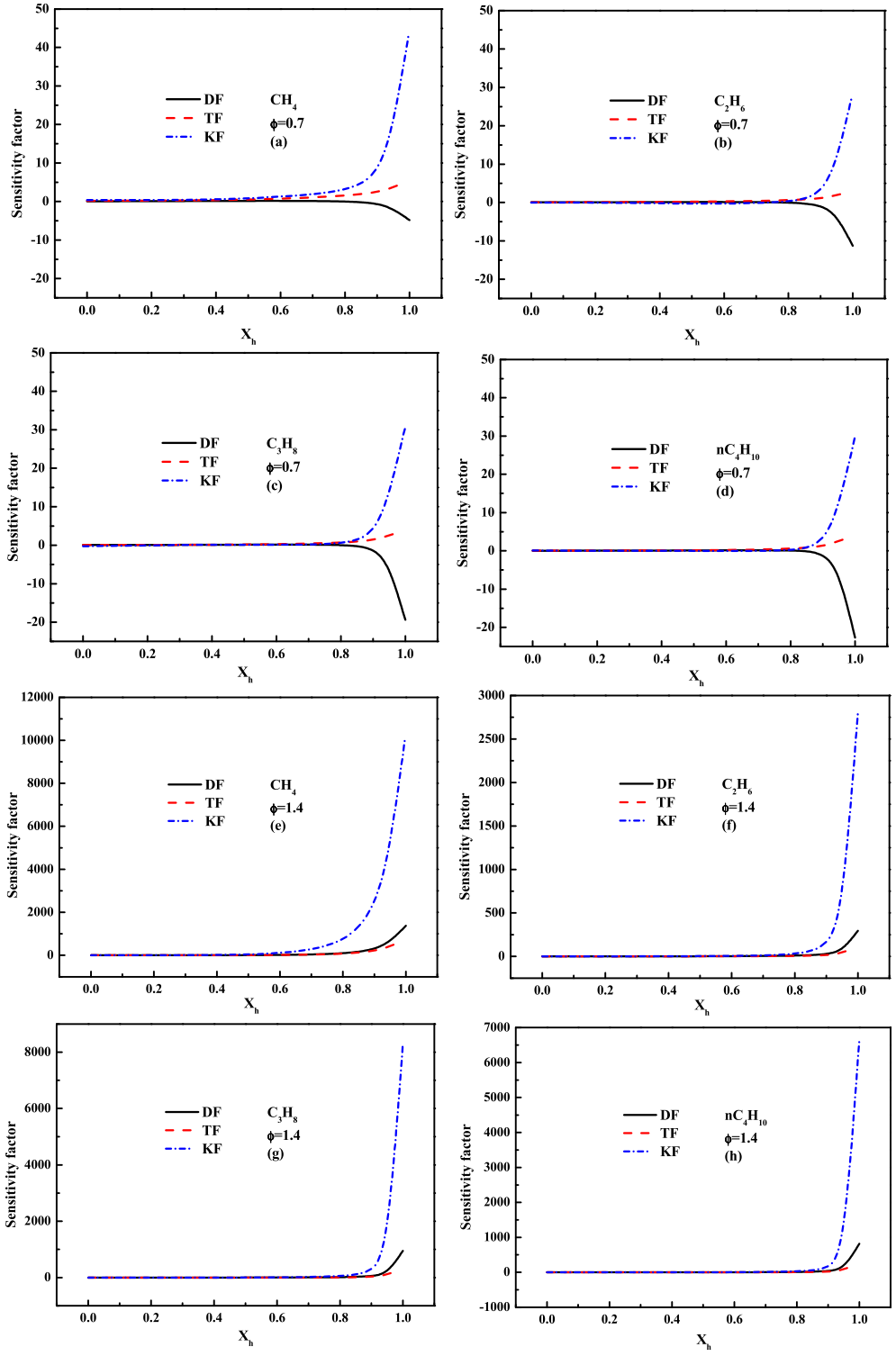

Fig. 9 – Sensitivity factors of C1–C4 n-alkane-hydrogen-air mixtures versus X_h at 1 atm and 298 K. (a) $\phi = 0.7$ for CH_4; (b) $\phi = 0.7$ for C_2H_6; (c) $\phi = 0.7$ for C_3H_8; (d) $\phi = 0.7$ for nC_4H_{10}; (e) $\phi = 1.4$ for CH_4; (f) $\phi = 1.4$ for C_2H_6; (g) $\phi = 1.4$ for C_3H_8; (h) $\phi = 1.4$ for nC_4H_{10}.

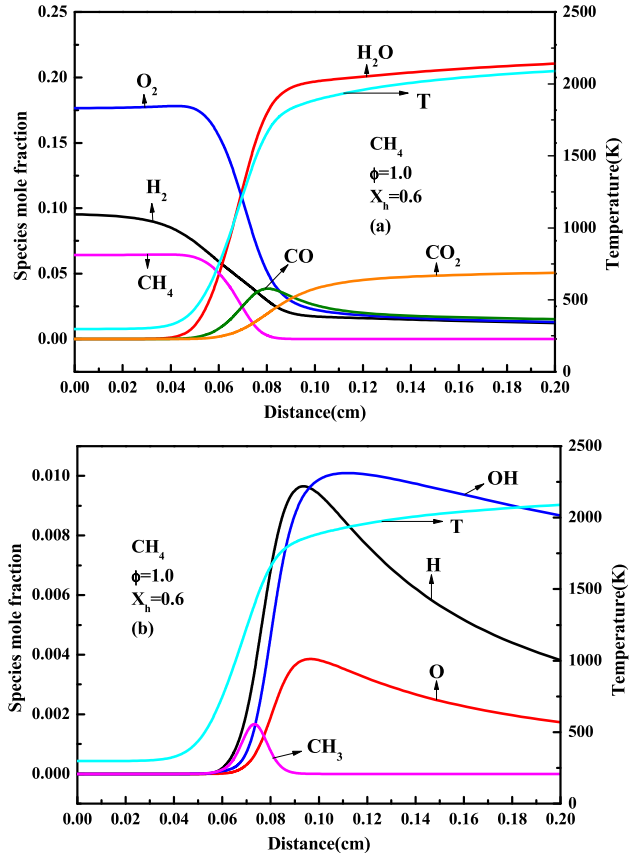

Fig. 10 – Predicted structure of premixed stoichiometric methane-hydrogen -air flame at 1 atm and 298 K ($X_h = 0.6$).

$$E_a = -2R\left[\frac{\partial(\ln \rho_u S_u^0)}{\partial(1/T_{ad})}\right]_p \quad (6)$$

In this work, the activation energy is obtained by perturbing the inert species (N_2) concentration.

The Markstein length can then be extracted from the following equation suggested by Bechtold and Matalon [39].

$$L_b = \delta_l\left[\sigma^{-1}\gamma_1 + \frac{1}{2}Ze(Le-1)\gamma_2\right] \quad (7)$$

where $\gamma_1 = 2\sigma/(\sqrt{\sigma}+1)$, $\gamma_2 = [4\sigma/(\sigma-1)][\sqrt{\sigma}-1-\ln(1/2)(\sqrt{\sigma}+1)]$ and σ is the expansion ratio. The Markstein number ($Ma = L_b/\delta_l$) can be then correspondingly derived and it quantifies to what extent the laminar flame speed is affected by the stretch.

Results and discussions

The global flame parameters

Figs. 1 and 2 show the calculated laminar flame speeds of C1–C4 n-alkane-hydrogen-air mixtures versus X_h under fuel lean, stoichiometric and fuel rich conditions. For the four alkanes-hydrogen mixtures studied here, the laminar flame speeds show the similar trend with increasing X_h. Specifically, when X_h is small, say 50% approximately, the increase in laminar flame speed due to hydrogen addition is very weak. When X_h is larger than 80%, the increase in laminar flame speed is significant. Additionally, although methane-air mixture has the lowest flame speed in the four alkane flames, the laminar flame speed of hydrogen

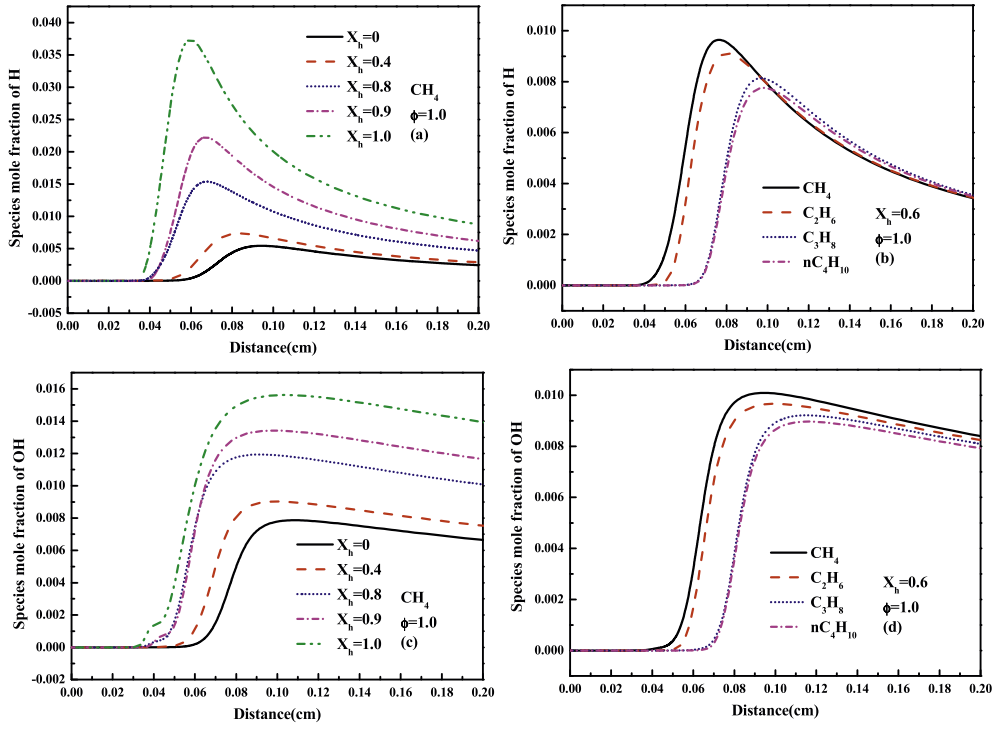

Fig. 11 – H and OH mole fractions of stoichiometric n-alkane-hydrogen flames with different X_h and carbon number at 1 atm and 298 K.

enriched methane is higher than other hydrogen-alkane mixtures when hydrogen fraction is sufficiently large, which indicates that the increase in flame speed due to hydrogen addition is more effective for methane, compared to other alkanes. Furthermore, the peak laminar flame speed of the fuel mixture shifts to the rich side with the increase of X_h.

Fig. 3 presents the adiabatic flame temperature of the C1–C4 n-alkane-hydrogen-air mixtures as a function of X_h under the fuel lean, stoichiometric and fuel rich conditions. The adiabatic flame temperature increases with the increase of X_h and reaches its maximum at $X_h = 1$. The adiabatic flame temperature shows the similar trend as the flame speed: when X_h is small, the increase in adiabatic flame temperature is weak; but when X_h is larger than 80%, the increase in adiabatic flame temperature is steep. However, the highest adiabatic flame temperature turns out to be under the stoichiometric condition, unlike the laminar flame speed dependence on the equivalence ratio. In addition, C2–C3 alkanes have similar adiabatic flame temperatures while methane has the lowest one compared with others, but shows faster increase with increasing X_h.

Fig. 4 presents the flame thickness δ_l of the C1–C4 n-alkane-hydrogen flame versus X_h. Flame thickness decreases with the increase of X_h, especially under the high hydrogen addition condition. For different equivalence ratios, the flame thickness shows the smallest change at the stoichiometric condition. When X_h is small, the methane–hydrogen mixture has the largest flame thickness and ethane–hydrogen mixture has the smallest one. When X_h is increased, the dependence of flame thickness on carbon number is gradually modified: the flame thickness of the n-butane-hydrogen becomes the highest, and that of the methane–hydrogen mixture becomes the smallest.

Fig. 5 displays the calculated Lewis number (*Le*) of C1–C4 n-alkane-hydrogen-air mixtures versus X_h at equivalence ratios of 0.7 and 1.4. As shown in Fig. 5a, *Le* decreases with the increase of X_h and the decreasing tendency becomes more apparent in high hydrogen fraction region at $\phi = 0.7$. At $\phi = 1.4$, *Le* increases with the increase of X_h and shows significant growth in the high X_h region. This phenomenon is resulted from the small molecular weight of hydrogen and the large mass diffusivity. This is consistent to the observations by Addabbo [40], when equivalence ratio increases from lean to rich, *Le* is increased for light fuels and decreased for heavy fuels. Thus, *Le* of hydrogen and methane flame is larger than unity under fuel rich conditions and smaller than unity under fuel lean conditions, while the C_2H_6, C_3H_8, n-C_4H_{10} flames show the reverse trends. For this reason, *Le* is decreased under fuel lean conditions and increased under fuel rich conditions with the increase of X_h.

Fig. 6 shows the Zeldovich number (*Ze*) versus X_h at equivalence ratios of 0.7 and 1.4. *Ze* decreases with hydrogen addition and shows a distinct drop in the large X_h region, indicating a similar trend for the global activation energy (E_a). This trend reflects the controlling effect of the adiabatic flame temperature, which increases with the increase of X_h especially in the large X_h region and facilitates the temperature-sensitive two body branching reactions relative to the temperature-insensitive three-body termination reactions

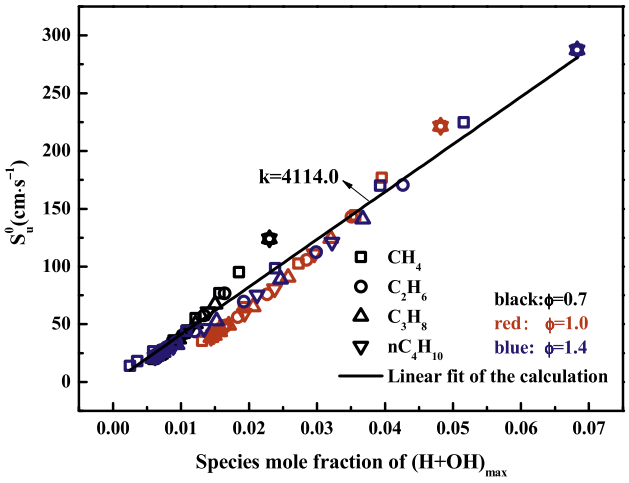

Fig. 12 – Laminar flame speed as functions of the maximum (H + OH) mole fraction in the reaction zone for C1–C4 n-alkane flames with different X_h and various equivalence ratios at 1 atm and 298 K: symbols for calculated data and lines for linear fit of the calculation.

[28,41], resulting in faster reaction with the increase of X_h. It can be seen that alkane flames presents smaller *Ze* in the fuel lean condition and hydrogen flame shows smaller *Ze* in the fuel rich condition, leading to a much more remarkable decrease with the increase of X_h for the rich fuel.

Fig. 7 shows the calculated Markstein number, *Ma*, of C1–C4 n-alkane-hydrogen-air mixtures versus X_h at equivalence ratios of 0.7 and 1.4. It can be seen that *Ma* decreases with the increase of X_h at $\phi = 0.7$ (Fig. 7a), however, at the equivalence ratio of 1.4, *Ma* increases and then decreases with the increase of X_h, giving its peak at X_h around 0.9 (Fig. 7b). The different trends of *Ma* for different equivalence ratios are mainly caused by the combined effect of *Ze* and *Le*. Under fuel

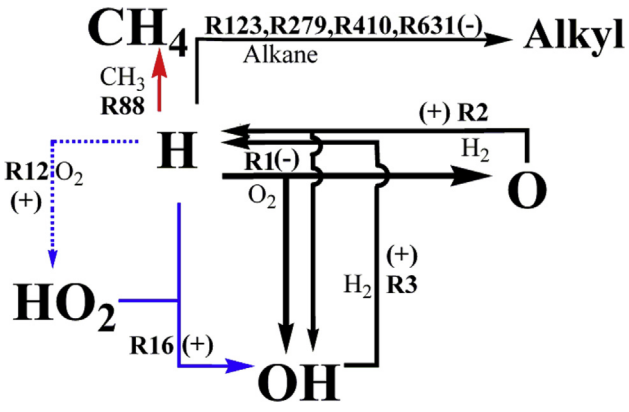

Fig. 13 – Main reaction pathways of H and OH radicals for C1–C4 n-alkane-hydrogen-air mixtures. Dotted line: pathway only effective with sufficiently large X_h; Solid lines: pathways effective with all X_h; Red lines: H consumption pathways enhanced at small X_h region; Blue lines: H consumption pathways enhanced at large X_h region. (For interpretation of the references to color in this figure legend, the reader is referred to the web version of this article.)

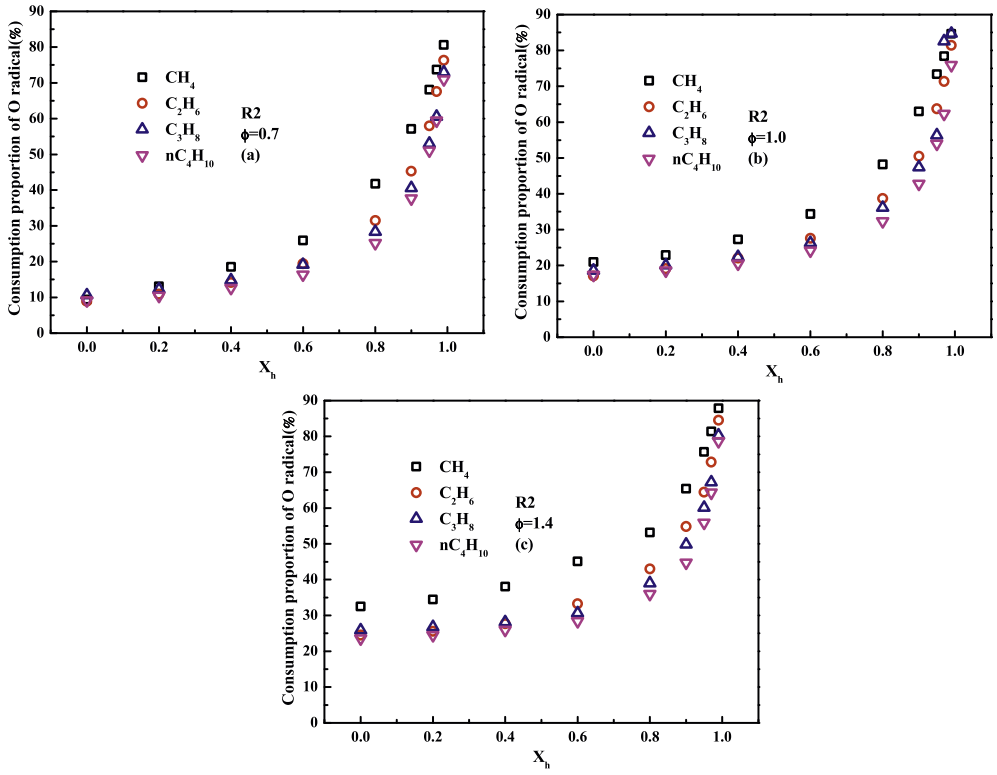

Fig. 14 – Consumption proportion of H radical from R2 at 1 atm and 298 K. (a) $\phi = 0.7$; (b) $\phi = 1.0$; (c) $\phi = 1.4$.

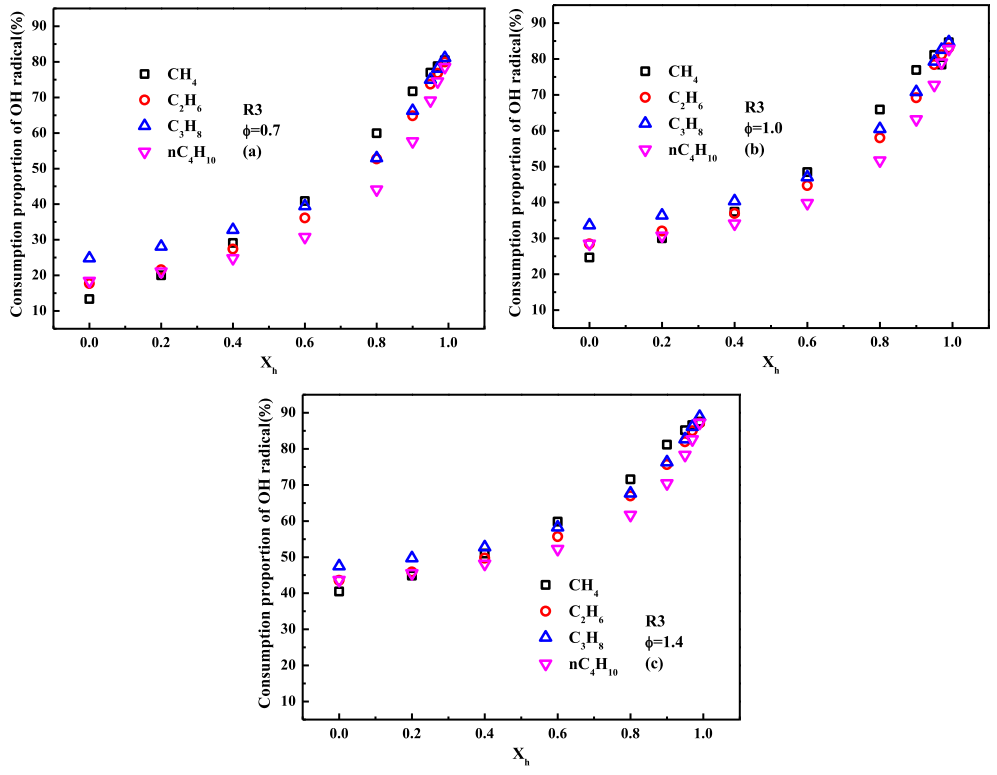

Fig. 15 – Consumption proportion of OH radical from R3 at 1 atm and 298 K. (a) $\phi = 0.7$; (b) $\phi = 1.0$; (c) $\phi = 1.4$.

lean condition, both *Le* and *Ze* are decreased with the increase of X_h, thus the *Ma* shows similar trend. Under fuel rich condition, *Le* increases with hydrogen addition while *Ze* shows a significant decrease. The net effect of *Le* and Ze contribute to the non-monotonic variation of *Ma* with X_h. The increasing trend of *Le* dominates in most range and *Ma* shows an increase in small X_h region, however, the significant drop of *Ze* becomes the dominant factor and results in the reversing trend of *Ma* in the large X_h region. Furthermore, the value of *Le* has a great influence on the sign of *Ma*. Under fuel lean condition, methane flame has negative *Ma* with all X_h while the others express positive value with small hydrogen addition. The main reason for this phenomenon is that methane and hydrogen have *Le* smaller than unity, so (*Le*-1) is negative while the *Le* of others are larger than unity with small X_h. Under fuel rich condition, methane presents higher value than others for the same reason.

Three factors on flame speed enhancement

Previous research [21,22] classified the methane-hydrogen flame into three regimes, namely the methane-dominated, the transition and the methane-inhibited hydrogen combustion regimes. They believe that the first and third one have linear trends with hydrogen addition. Fig. 8 gives the calculated growth rates of the normalized laminar flame speeds of C1–C4 n-alkane-hydrogen-air mixtures versus X_h. This parameter quantifies the extent of flame speed increase due to unit percent of hydrogen addition. It is seen that the growth rates of the normalized laminar flame speeds keep almost unchanged with small hydrogen addition, and at the large X_h region, the growth rates become extremely high. In order to interpret the increasing mechanisms of laminar flame speed due to hydrogen addition, theoretical analysis was conducted.

Based on the one step overall reaction assumption, the laminar flame speed is found to be correlated with the Lewis number, which represents the diffusion effect, the overall activation energy, which represents the kinetic effect and the adiabatic flame temperature which represents the thermal effect.

$$S_u^0 \sim (\alpha Le)^{1/2} \exp(-T_a/2T_{ad}) \tag{8}$$

where α is the thermal diffusivity and T_a ($=E_a/R$) is the activation temperature. The influence of diffusion can be treated as $(\alpha Le)^{1/2}$, and the effects of thermal and kinetic can be considered as a combined Arrhenius effects, represented by the exponential factor $\exp(-T_a/2T_{ad})$. To access the relative importance of these three aspects, we take derivative of the normalized laminar flame speed $S_u^0/S_u^0(0)$ with respect to X_h.

$$\frac{d(S_u^0/S_u^0(0))}{dX_h} = DF + TF + KF \tag{9}$$

$$DF = \frac{\exp(-T_a/2T_{ad})}{S_u^0(0)} \frac{d(\alpha Le)^{1/2}}{dX_h} \tag{10}$$

$$TF = \frac{(\alpha Le)^{1/2} \exp(-T_a/2T_{ad}) T_a}{2S_u^0(0)T_{ad}^2} \frac{dT_{ad}}{dX_h} \tag{11}$$

$$KF = -\frac{(\alpha Le)^{1/2} \exp(-T_a/2T_{ad})}{2S_u^0(0)T_{ad}} \frac{dT_a}{dX_h} \tag{12}$$

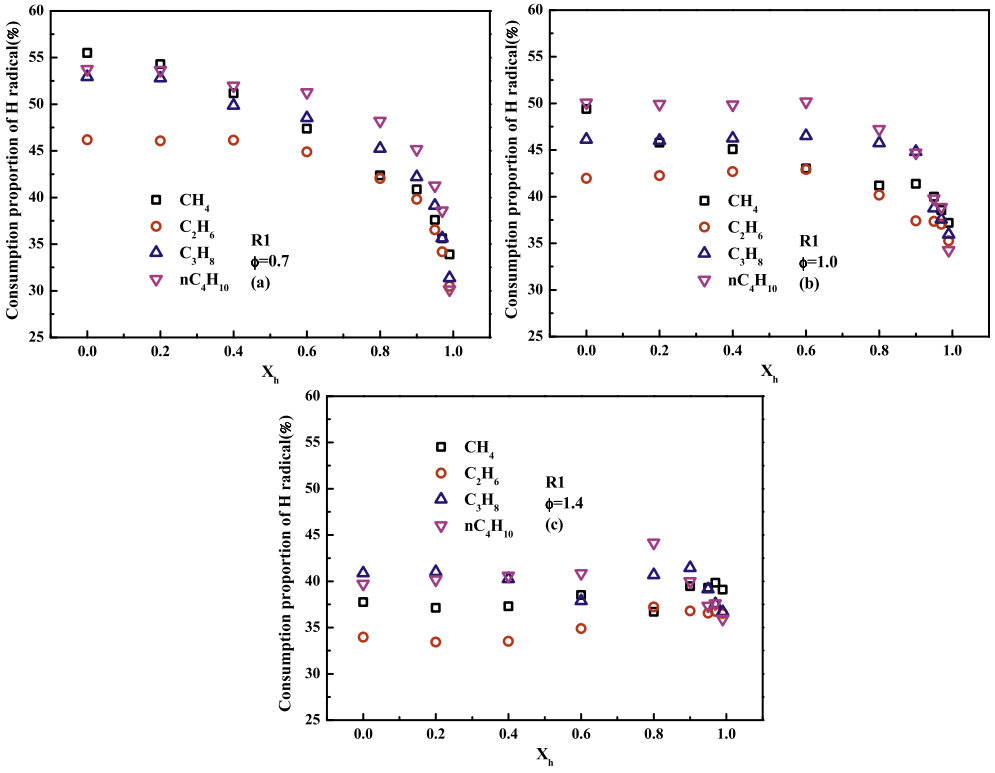

Fig. 16 – Consumption proportion of H radical from R1 at 1 atm and 298 K. (a) $\phi = 0.7$; (b) $\phi = 1.0$; (c) $\phi = 1.4$.

where DF, TF, KF are short for the diffusion, thermal and kinetic sensitivity factor, respectively. These three parameters qualitatively represent the modifications of the diffusion, thermal and kinetics due to hydrogen addition. Fig. 9 illustrates the sensitivity factor as a function of X_h. It is seen that in all cases the three sensitivity factors change little until hydrogen addition reaches a sufficiently high value. The great change of the three sensitivity factors agrees well with the remarkable increase of laminar flame speeds in the large X_h region. In addition, at $\phi = 0.7$, the thermal and kinetic sensitivity factors increase with hydrogen addition, indicating a promoting effect on the laminar flame speed; while the diffusion factor decreases from the decrease of *Le* with hydrogen addition, leading to a suppression effect on the flame speed enhancement. At $\phi = 1.4$, *Le* increases with hydrogen addition so that the diffusion sensitivity has an increasing trend in addition to the thermal and kinetic ones, indicating a greater promotion of laminar flame speeds. Considering the different trends of diffusion factor under different conditions, the combined effects of these three factors can explain the greater growth of laminar flame speeds under the fuel-rich condition than under the fuel-lean condition. Furthermore, it can be seen that the kinetic factor plays the most important role on the enhancement of laminar flame speed.

Kinetic analysis

The above analysis based on one step overall reaction assumption shows the importance of the chemical kinetics induced by hydrogen addition. However, the overall activation energy is just a global overall reactivity for given mixture and it does not represent the real chemical kinetics in flames. Thus in the following, the detailed chemical kinetics were analyzed, including the chemical flame structure, sensitivity analysis and reaction path analysis.

Flame structure

The structures of premixed stoichiometric methane-hydrogen-air flame ($X_h = 0.6$) is explored in Fig. 10. Profiles of the stable species (H_2, CH_4, O_2, H_2O, CO, CO_2, etc) are presented in Fig. 10a, and that of radical species are provided in Fig. 10b. The reactants (H_2, CH_4, O_2) are decreased and final products (H_2O, CO_2) show increasing trends while the intermediate product (CO) first increases and then decreases with the distance through the flame as expected. Besides, the flame temperature increases along the distance. In this case, the OH radical has the largest concentration in the flame, compared to other free radicals such as H and O radicals. The CH_3 radical shows the lower concentration.

The fractions of H and OH radicals vary with hydrogen fraction significantly, as shown in Fig. 11. It can be seen that different alkanes show similar tendencies of H and OH radicals thus we use CH_4 to interpret the hydrogen addition effect on flame structures. It is seen that both H and OH radicals increase by hydrogen addition and the increasing trend is more significant at the high X_h region. Moreover, H radical increases faster than OH radical by hydrogen addition and domains in the large X_h region. This is because that H_2 is mainly consumed by two reactions, namely the reaction R2 ($O + H_2 = H + OH$) and R3 ($OH + H_2 = H + H_2O$). R2 produces both H and OH while R3 only produces H. Besides, R3 accounts for a larger proportion in the H_2 consumption, about 70% and

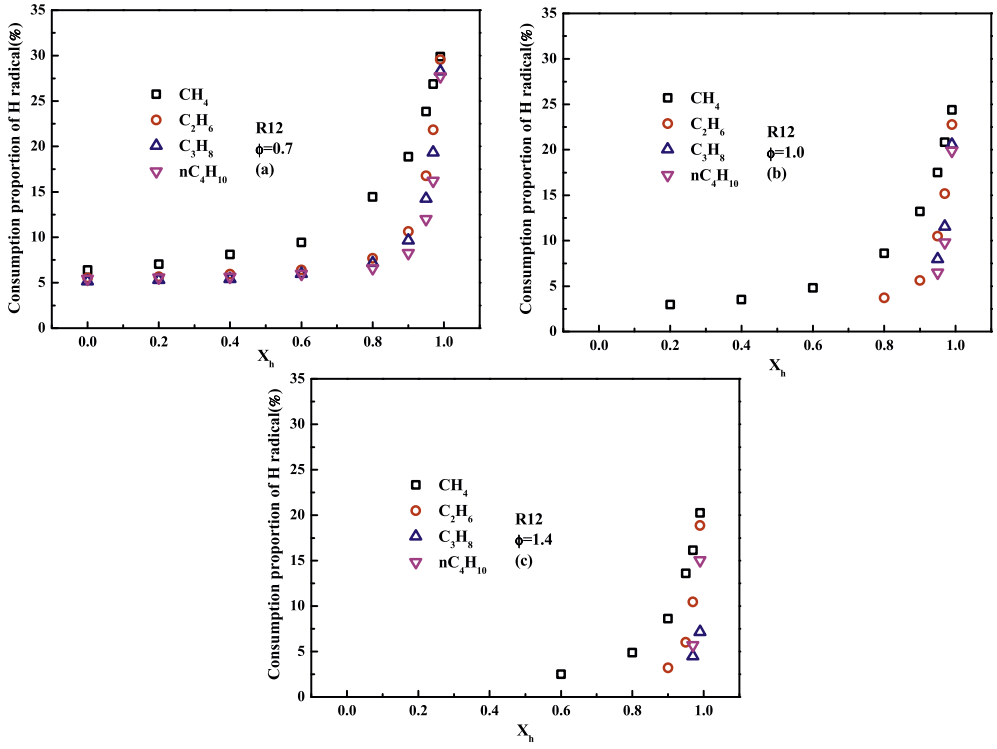

Fig. 17 – Consumption proportion of H radical from R12 at 1 atm and 298 K. (a) $\phi = 0.7$; (b) $\phi = 1.0$; (c) $\phi = 1.4$.

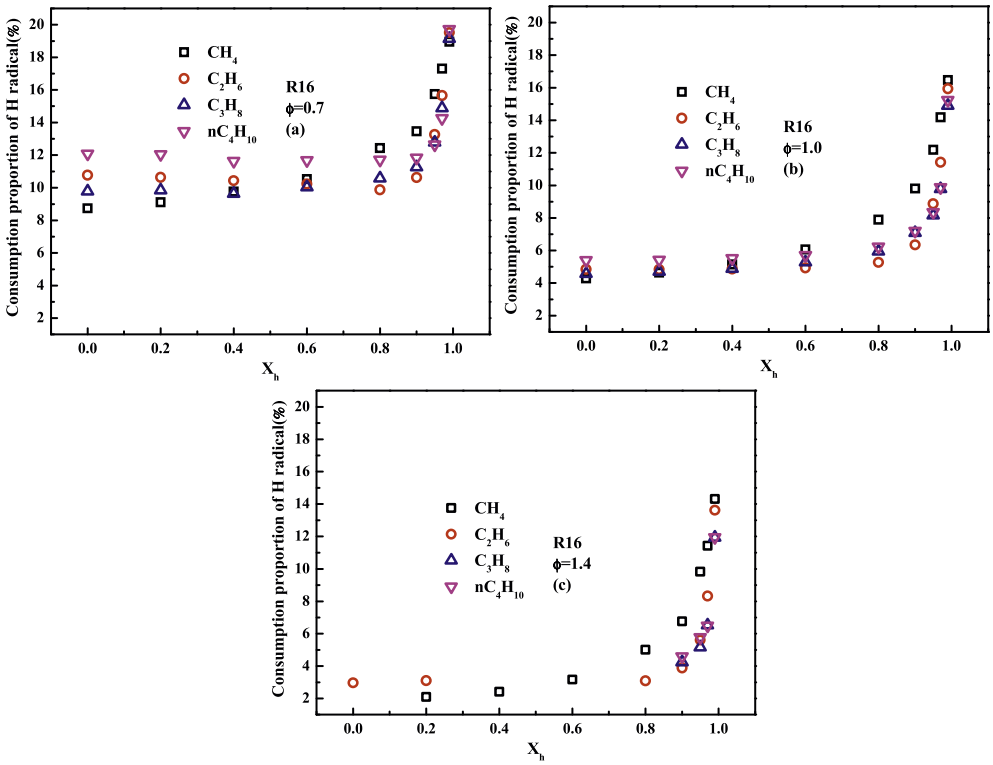

Fig. 18 – Consumption proportion of H radical from R16 at 1 atm and 298 K. (a) $\phi = 0.7$; (b) $\phi = 1.0$; (c) $\phi = 1.4$.

R2 only about 30%. Resulting from the different production and proportion of R2 and R3, H radical shows a more significant increase than OH radical by hydrogen addition.

Reaction path analysis

Sensitivity analysis with different equivalence ratios and alkanes show that the reactions with high sensitivity coefficients are mainly related to the H and OH radicals, indicating the importance of the free radical H and OH in the laminar flame speed prediction. Fig. 12 shows the laminar flame speed versus the maximum (H + OH) mole fraction, which means "max[X(H) + X(OH)]" at a certain location in the reaction zone. It can be obviously seen that the laminar flame speed for all mixtures correlate quasi-linearly with the maximum (H + OH) mole fraction. This empirical correlation is shown as.

$$S_u^0 = k[H + OH]_{max} cm \cdot s^{-1} \quad (13)$$

where k is the coefficient that represents the sensitivity of laminar flame speed to the maximum (H + OH) mole fraction and the value of k is given in Fig. 12.

Further analysis on the consumption/production of H and OH radicals were conducted since the above empirical correlation indicates the importance of these two radicals for the laminar flame speed prediction. Fig. 13 shows that the main reaction channels involving the H and OH radicals are:

R1. $H + O_2 = O + OH$

R2. $O + H_2 = H + OH$

R3. $OH + H_2 = H + H_2O$

R12. $H + O_2 (+M) = HO_2 (+M)$

R16. $HO_2 + H = OH + OH$

R88. $CH_3 + H (+M) = CH_4 (+M)$

R123. $CH_4 + H = CH_3 + H_2$

R279. $C_2H_6 + H = C_2H_5 + H_2$

R410. $C_3H_8 + H = iC_3H_7 + H_2$

R631. $C_4H_{10} + H = sC_4H_9 + H_2$

In Fig. 13, the pathways with '+' and '−' respectively represent the favored and unfavored channels with the increase of hydrogen addition. The dotted line indicates the pathway of R12 which is only effective with sufficiently large X_h. Rate of consumption of different species was calculated by the Chemkin II and then the consumption of a specific species through the individual reactions was calculated by the spatial integration of the elementary reaction rate of consumption within the whole

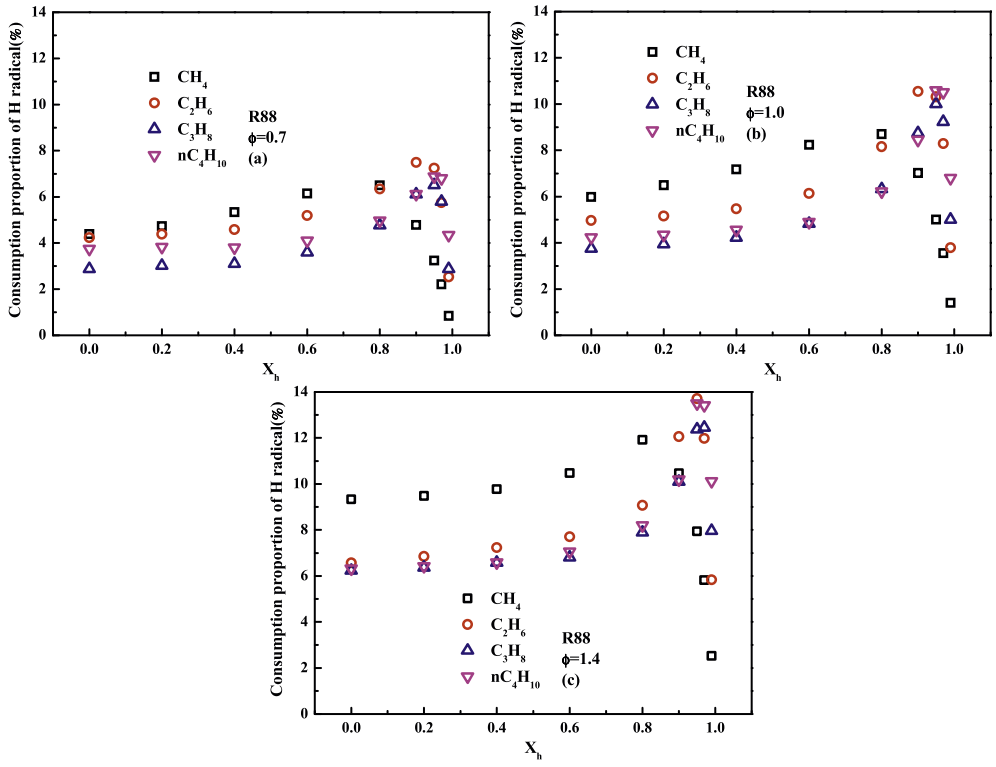

Fig. 19 – Consumption proportion of H radical from R88 at 1 atm and 298 K. (a) $\phi = 0.7$; (b) $\phi = 1.0$; (c) $\phi = 1.4$.

reaction zone [42,43]. The specific consumption proportions (rate of consumption of a specific species through the individual reaction normalized by the total rate of consumption of the specific species) are shown later in Figs. 14 to 20. It is seen that the four alkane-hydrogen mixtures studied here show very similar major pathways of H and OH production/consumption; we then attempt to explore the kinetic mechanisms for the enhanced reactivity (increased laminar flame speed) due to hydrogen addition. Firstly, the production of H radical is mainly contributed from R2 ($O + H_2 = H + OH$) and R3 ($OH + H_2 = H + H_2O$). These two H production channels are favored with the increase of hydrogen addition. Because of the increased consumption of O and OH respectively through R2 and R3 (see Figs. 14 and 15), H radical production is increased by hydrogen addition. Secondly, the consumption of H is primarily through the main chain branching channel R1 and this channel is unfavored with the increase of hydrogen addition, and H rate of consumption from R1 decreases remarkably at large X_h region (50–30%, see Fig. 16). Furthermore, the reactions of H abstraction from alkanes, say R123 ($CH_4 + H = CH_3 + H_2$), R279 ($C_2H_6 + H = C_2H_5 + H_2$), R410 ($C_3H_8 + H = H_2 + iC_3H_7$) and R631 ($C_4H_{10} + H = sC_4H_9 + H_2$) shows similar trends with R1, but their contributions are weaker than R1 (less than 30%, see Fig. 20); R12 ($H + O_2 (+M) = HO_2 (+M)$) consumes negligible H radicals at small X_h region, but it becomes effective when X_h is sufficiently large. When HO_2 is accumulated to a sufficient concentration at the large X_h region, the subsequent reaction R16 ($HO_2 + H = OH + OH$) becomes important (see Fig. 18) to produce OH radicals and favors the reactivity. The contribution of R88 ($CH_3 + H (+M) = CH_4 (+M)$) increases gently first when X_h is small, and it then decreases dramatically with the increase of X_h.

If we artificially divide the hydrogen addition level into the "small X_h" and "large X_h" region, the kinetic reason for the laminar flame speed enhancement due to hydrogen addition is summarized as the following:

In the small X_h region, as shown in Fig. 13, the chain branching reaction (promoting reactions) R1 dominates the H consumption, yet its contribution decreases with the increase of X_h. The H abstraction reactions from alkane fuel (R123, R279, R410, and R631) are chain propagating but reduce the reactivity. These reactions also contribute to the H consumption. The termination reaction R88 also presents a moderate contribution to H consumption and its contribution grows with the increase of X_h. Because the consumption proportion from R12 is small and that from R16 changes little in the small X_h region, the two reactions are not considered in this region. Thus the gentle increase of the laminar flame speed in this small X_h region (observed in Fig. 1) is from the competition of H radical between the chain branching reaction R1 and the H abstraction reactions as well as the termination reaction R88. Specifically, the amount of H and OH radicals increases with the hydrogen addition, which leads to an increased reactivity. However, R88 produces stable species CH_4 and no active radicals, thus it increases H consumption proportion, compared to R1 which produces OH and O radicals, slows down the H and OH radical accumulation by hydrogen addition.

In the large X_h region, R12 ($H + O_2 (+M) = HO_2 (+M)$) becomes effective in consuming H radical, as shown by the dotted pathway in Fig. 13. However, when HO_2 is accumulated to a sufficient concentration, the subsequent chain branching R16 ($HO_2 + H = OH + OH$), which is not sensitive at the small X_h region, is activated. R16 favors the reactivity and this sequence has

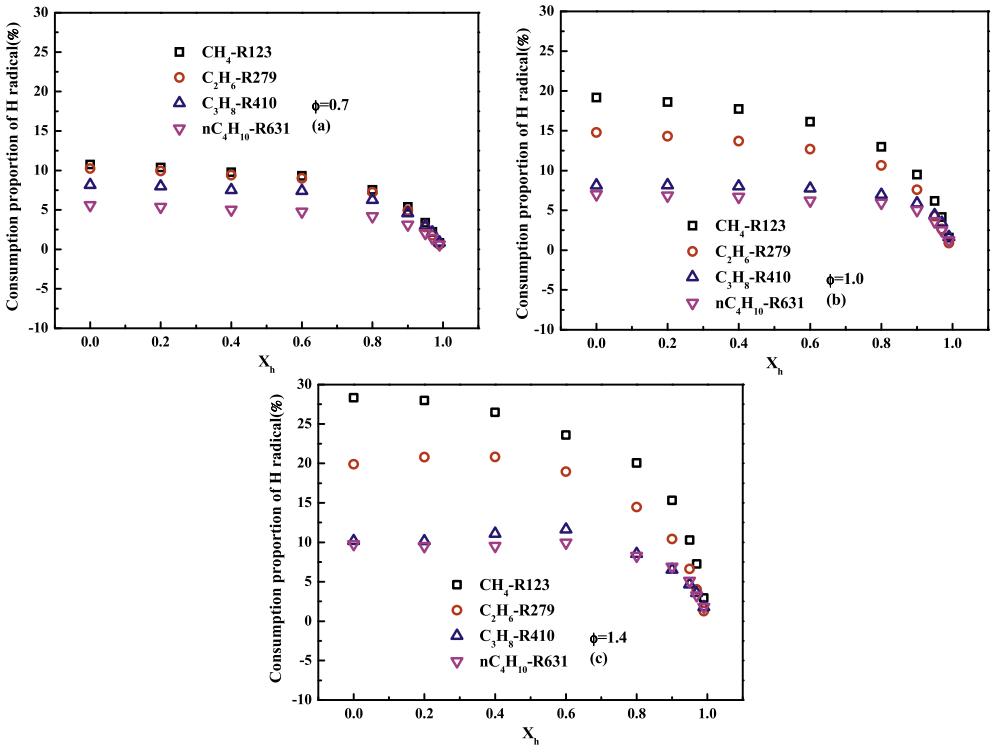

Fig. 20 – Consumption proportion of H radical from alkane H abstraction reactions at 1 atm and 298 K. (a) $\phi = 0.7$; (b) $\phi = 1.0$; (c) $\phi = 1.4$.

been previously reported by Dagaut and Nicolle [44] for natural gas/hydrogen oxidation in a jet stirred reactor study. Additionally, at the large X_h region, the contributions from R88, R1 and the alkane H abstraction reactions are significantly decreased, and more H radical is consumed through the R12/R16 sequence, resulting in the remarkable growth of (H + OH) concentration at the large X_h region and consequently a rapid increase in laminar flame speeds with the increase of X_h as shown in Fig. 8.

It is noted that for the dependence of the equivalence ratio, the H abstraction reaction of alkanes (R123, R279, R410, and R631) have an increasing trend (see Fig. 20). This phenomenon is reasonable because the abundant oxygen under the fuel lean condition indicates that more fuel is consumed by OH and O while H radical shows a priority in fuel consumption under the fuel rich condition. Similar behaviors of OH radical for lean methane-air mixtures consumption have been reported in previous researches [21,44,45]. The abundant O_2 is responsible for the larger proportion of R12 under the fuel lean condition. Consequently, R12 is promoted in this case. In comparison, the consumption proportion of R88 increases with the equivalence ratio and changes more quickly under fuel rich condition. Furthermore, methane shows a variation of kinetic reaction path with smaller amount of hydrogen addition compared with other alkanes, which is consistent with the laminar flame speed behavior.

Conclusions

Numerical simulations of the laminar premixed C1–C4 n-alkanes with different hydrogen addition levels (X_h) were conducted using the USC II. Flame parameters, including laminar flame speeds, adiabatic flame temperature (T_{ad}), flame thickness (δ_l), Lewis number (*Le*), Zeldovich number (*Ze*) and Markstein number (*Ma*) were calculated at different hydrogen additions and equivalence ratios. Results show that all the flame parameters are altered with the increase of X_h, and their dependence on X_h becomes increasingly significant at the high X_h region. Based one step overall assumption, the increase of laminar flame speeds by hydrogen addition is interpreted through three factors: the overall activation energy which represents the kinetic effect, the adiabatic flame temperature which represents the thermal effect and the global Lewis number which represents the diffusion effect. Qualitative comparisons among the three factors indicate that kinetic effect is the most prominent. Detailed kinetic analysis was conducted by looking into the flame structures and it shows that laminar flame speeds of all mixtures can be linearly correlated with the maximum mole fraction of (H + OH). To further understand the kinetic effect of hydrogen addition, the reaction flux and rate of consumption of key radicals show that the kinetic effect of hydrogen addition differs at small and large X_h regions. Although the amount of H and OH radicals increases with the increase of X_h, the consumption proportion of H radical from R88 (CH_3+H(+M) = CH_4 (+M)) is increased, and the consumption proportion of H radical from R1 (H + O_2 = O + OH) is decreased at the small X_h region, leading to a comparatively weaker increase in laminar flame speeds by hydrogen addition in this region. At the large X_h region, the consumption proportion of H radical from R88 decreases dramatically, and the chain sequence R12 (H + O_2(+M) = HO_2(+M))/R16 (HO_2+H = OH + OH) which is not

important at small X_h region is activated and the increased production OH radicals lead to the remarkable increase of laminar flame speed.

Acknowledgment

This work is supported by the National Natural Science Foundation of China (51206131, 51136005, 51121092), and the National Basic Research Program of China (2013CB228406). Support from the Fundamental Research Funds for the Central Universities is also appreciated.

REFERENCES

[1] Calcote H, Gregory C, Barnett C, Gilmer RB. Spark ignition. Effect of molecular structure. Ind Eng Chem 1952;44:2656–62.
[2] Tang C, Zhang Y, Huang Z. Progress in combustion investigations of hydrogen enriched hydrocarbons. Renew Sust Energ Rev 2014;30:195–216.
[3] Wierzba I, Kilchyk V. Flammability limits of hydrogen–carbon monoxide mixtures at moderately elevated temperatures. Int J Hydrogen Energy 2001;26:639–43.
[4] Zebetakis MG. Flammability characteristics of combustible gases and vapors. U. S Bur Mines Bull 1965:627.
[5] Liu DDS, MacFarlane R. Laminar burning velocities of hydrogen–air and hydrogen air–steam flames. Combust Flame 1983;49:59–71.
[6] Lamoureux N, Paillard CE. Natural gas ignition delay times behind reflected shock waves: application to modelling and safety. Shock Waves 2003;13:57–68.
[7] Mariani A, Prati MV, Unich A, Morrone B. Combustion analysis of a spark ignition i. c. engine fuelled alternatively with natural gas and hydrogen–natural gas blends. Int J Hydrogen Energy 2013;38:1616–23.
[8] Kahraman N, Ceper B, Akansu S, Aydin K. Investigation of combustion characteristics and emissions in a spark-ignition engine fuelled with natural gas–hydrogen blends. Int J Hydrogen Energy 2009;34:1026–34.
[9] Akansu SO, Dulger Z, Kahraman N, Veziroğlu TN. Internal combustion engines fueled by natural gas-hydrogen mixtures. Int J Hydrogen Energy 2004;29:1527–39.
[10] Rakopoulos CD, Scott MA, Kyritsis DC, Giakoumis EG. Availability analysis of hydrogen/natural gas blends combustion in internal combustion engines. Energy 2008;33:248–55.
[11] Huang Y, Yang V. Dynamics and stability of lean-premixed swirl-stabilized combustion. Prog Energy Combust Sci 2009;35:293–364.
[12] Zhang Y, Huang Z, Wei L, Zhang J, Law CK. Experimental and modeling study on ignition delays of lean mixtures of methane, hydrogen, oxygen, and argon at elevated pressures. Combust Flame 2012;159:918–31.
[13] Tang C, Man X, Wei L, Pan L, Huang Z. Further study on the ignition delay times of propane–hydrogen–oxygen–argon mixtures: effect of equivalence ratio. Combust Flame 2013;160:2283–90.
[14] Pan L, Zhang Y, Zhang J, Tian Z, Huang Z. Shock tube and kinetic study of $C_2H_6/H_2/O_2$/Ar mixtures at elevated pressures. Int J Hydrogen Energy 2014;39:6024–33.
[15] Herzler J, Naumann C. Shock-tube study of the ignition of methane/ethane/hydrogen mixtures with hydrogen contents from 0% to 100% at different pressures. Proc Combust Inst 2009;32:213–20.
[16] Gersen S, Anikin N, Mokhov A, Levinsky H. Ignition properties of methane/hydrogen mixtures in a rapid compression machine. Int J Hydrogen Energy 2008;33:1957–64.
[17] Zhang Y, Jiang X, Wei L, Zhang J, Tang C, Huang Z. Experimental and modeling study on auto-ignition characteristics of methane/hydrogen blends under engine relevant pressure. Int J Hydrogen Energy 2012;37:19168–76.
[18] Law C. Effects of hydrocarbon substitution on atmospheric hydrogen–air flame propagation. Int J Hydrogen Energy 2004;29:867–79.
[19] Yu G, Law CK, Wu CK. Laminar flame speeds of hydrocarbon air mixtures with hydrogen addition. Combust Flame 1986;63(3):339–47.
[20] Ren JY, Qin W, Egolfopoulos FN, Tsotsis TT. Strain-rate effects on hydrogen-enhanced lean premixed combustion. Combust Flame 2001;124:717–20.
[21] Hu E, Huang Z, He J, Jin C, Zheng J. Experimental and numerical study on laminar burning characteristics of premixed methane–hydrogen–air flames. Int J Hydrogen Energy 2009;34:4876–88.
[22] Disarli V, Benedetto A. Laminar burning velocity of hydrogen–methane/air premixed flames. Int J Hydrogen Energy 2007;32:637–46.
[23] Halter F, Chauveau C, Djebaïli-Chaumeix N, Gökalp I. Characterization of the effects of pressure and hydrogen concentration on laminar burning velocities of methane–hydrogen–air mixtures. Proc Combust Inst 2005;30(1):201–8.
[24] Hermanns RTE, Konnov AA, Bastiaans RJM, de Goey LPH, Lucka K, Köhne H. Effects of temperature and composition on the laminar burning velocity of $CH_4+H_2+O_2+N_2$ flames. Fuel 2010;89:114–21.
[25] Miao H, Ji M, Jiao Q, Huang Q, Huang Z. Laminar burning velocity and Markstein length of nitrogen diluted natural gas/hydrogen/air mixtures at normal, reduced and elevated pressures. Int J Hydrogen Energy 2009;34:3145–55.
[26] Hu E, Huang Z, He J, Miao H. Experimental and numerical study on lean premixed methane–hydrogen–air flames at elevated pressures and temperatures. Int J Hydrogen Energy 2009;34:6951–60.
[27] Wu F, Kelley AP, Tang C, Zhu D, Law CK. Measurement and correlation of laminar flame speeds of CO and C2 hydrocarbons with hydrogen addition at atmospheric and elevated pressures. Int J Hydrogen Energy 2011;36(20):13171–80.
[28] Tang C, Huang Z, Jin C, He J, Wang J, Wang X, et al. Laminar burning velocities and combustion characteristics of propane–hydrogen–air premixed flames. Int J Hydrogen Energy 2008;33:4906–14.
[29] Tang C, He J, Huang Z, Jin C, Wang J, Wang X, et al. Measurements of laminar burning velocities and Markstein lengths of propane–hydrogen–air mixtures at elevated pressures and temperatures. Int J Hydrogen Energy 2008;33:7274–85.
[30] Tang CL, Huang ZH, Law CK. Determination, correlation, and mechanistic interpretation of effects of hydrogen addition on laminar flame speeds of hydrocarbon–air mixtures. Proc Combust Inst 2011;33:921–8.
[31] Sher E, Ozdor N. Laminar burning velocities of n-butane/air mixtures enriched with hydrogen. Combust Flame 1992;89:214–20.
[32] Huang Z, Zhang Y, Zeng K, Liu B, Wang Q, Jiang D. Measurements of laminar burning velocities for natural gas–hydrogen–air mixtures. Combust Flame 2006;146:302–11.
[33] Kee RJ, Grcar JF, Smooke MD, Miller JA. A fortran program for modeling steady laminar one-dimensional premixed flames. Report SAND85–8240. Sandia National Laboratories; 1985.

[34] Kee RJ, Rupley FM, Miller JA. Chemkin-II: a fortran chemical kinetics package for the analysis of gas-phase chemical kinetics. Sandia Report SAND89–8009. Sandia National Laboratories; 1989.
[35] Wang H, You X, Joshi AV, Davis SG, Laskin A, Egolfopoulos FN, et al. USC mech version II. High-temperature combustion reaction model of H_2/CO/C1–C4 compounds. 2007. available at, http://ignis.usc.edu/USC_Mech_II.htm.
[36] Law CK, Jomaas G, Bechtold JK. Cellular instabilities of expanding hydrogen/propane spherical flames at elevated pressures: theory and experiment. Proc Combust Inst 2005;30:159–67.
[37] Law CK, Sung CJ. Structure, aerodynamics, and geometry of premixed flamelets. Prog Energy Combust Sci 2000;26:459–505.
[38] Law CK. Combustion physics. New York: Cambridge University Press; 2006.
[39] Bechtold JK, Matalon M. The dependence of the Markstein length on stoichiometry. Combust Flame 2001;127:1906–13.
[40] Addabbo R, Bechtold JK, Matalon M. Wrinkling of spherically expanding flames. Proc Combust Inst 2002;29:1527–35.
[41] Jomaas G, Law CK, Bechtold JK. On transition to cellularity in expanding spherical flames. J Fluid Mech 2007;583:1–26.
[42] Warnatz J. The structure of laminar alkane-, alkene-, and acetylene flames. Proc Combust Inst 1981;18:369–84.
[43] Das AK, Kumar K, Sung C-J. Laminar flame speeds of moist syngas mixtures. Combust Flame 2011;158:345–53.
[44] Dagaut P, Nicolle A. Experimental and detailed kinetic modeling study of hydrogen-enriched natural gas blend oxidation over extended temperature and equivalence ratio ranges. Proc Combust Inst 2005;30:2631–8.
[45] Ren JY, Qin W, Egolfopoulos FN, Mak H, Tsotsis TT. Methane reforming and its potential effect on the efficiency and pollutant emissions of lean methane–air combustion. Chem Eng Sci 2001;56:1541–9.